01 Feb 2001

Comparison of Single- and Two-Bubble Class Gas-Liquid Recirculation Models - Application to Pilot-Plant Radioactive Tracer Studies during Methanol Synthesis

Puneet Gupta

Muthanna H. Al-Dahhan
Missouri University of Science and Technology, aldahhanm@mst.edu

Milorad P. Dudukovic

Bernard A. Toseland

Recommended Citation

Comparison of single- and two-bubble class gas–liquid recirculation models — application to pilot-plant radioactive tracer studies during methanol synthesis

Puneet Gupta[a], Muthanna H. Al-Dahhan[a], Milorad P. Dudukovic[a,*], Bernard A. Toseland[b]

[a]*Chemical Reaction Engineering Laboratory (CREL), Department of Chemical Engineering, Campus Box 1198, Washington University St. Louis, MO 63130-4899, USA*
[b]*Air Products & Chemicals, Inc., PO Box 25780, Lehigh Valley, PA 18007, USA*

Abstract

Radioactive gas tracer measurements conducted during liquid-phase methanol synthesis from syngas in a pilot-scale slurry bubble column at the alternate fuels development unit (AFDU), La Porte have been compared with simulations from two mechanistic reactor models — single-bubble class model (SBCM) and two-bubble class model (TBCM). The model parameters are estimated from an independent sub-model gas and liquid recirculation, and the long-time-averaged slip velocity between the gas and liquid/slurry in the column center can be as high as 50–60 cm/s depending on the operating conditions. Comparison of experimental data with simulation results from the two models indicates that accurate description of interphase gas–liquid mass transfer is crucial to the reliable prediction of tracer responses. Coupled with a correct description of gas and liquid recirculation, the models presented here provides a simple and fundamentally based methodology for design and scale-up of bubble column reactors. © 2001 Published by Elsevier Science Ltd.

Keywords: Gas–liquid recirculation; Slurry bubble column; Mechanistic reactor modeling; Radioactive tracer studies

1. Introduction

The chemical industry places demands on operating bubble column reactors at high superficial gas velocities under high pressures and in large diameter vessels, especially in processes like the Fischer–Tropsch synthesis of liquid hydrocarbons or liquid-phase methanol production that are viewed as alternate sources of fuels/chemicals from synthesis gas. Under these conditions, bubble columns operate in the *churn-turbulent* regime characterized by frequent bubble coalescence and breakage and a nearly chaotic two-phase system. The characterization of the extent of gas and liquid/slurry phase mixing in these reactors is very critical to their proper design and scale-up.

Traditionally, the axial dispersion model (ADM) with interface mass transport has been used to describe the degree of backmixing in both phases and has been the basis for design of bubble and slurry bubble column reactors. Kastanek, Zahradnik, Kratochvil and Cermak (1993) have presented a detailed review of the correla-tions available for estimating the gas as well as liquid-phase effective dispersion coefficients pertinent to the ADM. However, these correlations are mostly empirical and do not provide reliable estimates for design and scale-up purposes. One of the reasons for the poor predictive capabilities of these correlations is that the ADM is suitable only for modeling of mixing processes in which the flow is not far away from ideal plug-flow conditions. Therefore, for recirculation dominated convective flows, such as those occurring during bubble column operation, the application of the ADM to describe the state of mixing is without a firm physical basis and has had limited success only in fitting the experimental data. Degaleesan, Dudukovic', Bhatt and Toseland (1996a) presented in detail the shortcomings of the ADM applied to gas tracer data from a pilot-scale slurry bubble column during liquid-phase methanol synthesis at the La Porte alternate fuels development unit (AFDU). It was shown that the gas and liquid-phase dispersion coefficients fitted to the tracer responses measured at various elevations did not exhibit a consistent trend and the values were widely scattered around the estimated means. Moreover, attempts to extract other parameters from the

---

* Corresponding author.

tracer data, such as volumetric mass transfer coefficients, did not seem to produce any consistent results. It was subsequently shown in a separate study that the liquid-phase mixing can be predicted in excellent agreement with experimental data using a two-compartment mechanistic model (Degaleesan, Roy, Kumar & Dudukovic', 1996b; Degaleesan, 1997), which accounted for mixing dominated by convective recirculation. Degaleesan and Dudukovic (1998) also derived the relationship between the axial dispersion coefficient and the parameters of the phenomenological recirculation and eddy diffusion model and explained the difficulties involved in obtaining a predictive axial dispersion coefficient.

The study of mixing in the gas phase, however, has still not received much attention, with the ADM being used for lack of better alternatives. Some models describe the gas phase dynamics in terms of "small" and "large" bubble classes resulting from a bimodal distribution of bubble sizes (Vermeer & Krishna, 1981; Shah, Kelkar, Godbole & Deckwer, 1982). These two classes of bubbles were shown to coalesce and interact frequently with each other resulting in higher mass transfer rates (de Swart, 1996). However, these models do not account for the effect of gas and liquid recirculation and the accompanying turbulence responsible for majority of the ensuing mixing. Given the inherent inadequacies of the ADM in describing gas backmixing in bubble column flows, phenomenological gas and liquid recirculation models have been developed as part of this study. The basis for these models is the liquid and gas recirculation resulting from the radial gas holdup distribution supported by extensive experimental database from the non-invasive measurement techniques consisting of computed tomography-CT and computer automated radioactive particle tracking-CARPT (Devanathan, Moslemian & Dudukovic, 1990; Kumar, Moslemian & Dudukovic, 1997; Degaleesan, 1997; Chen et al., 1998).

The first of the models is the two-bubble class model (TBCM), which is based on the assumption that the gas phase dynamics and recirculation are described by the presence of two-bubble classes — a "small" bubble class and a "large" bubble class, with the interaction between the two being modeled using an exchange coefficient, K (1/s). However, the assumption of a bimodal bubble size distribution still needs to be tested at operating conditions of interest, and therefore, a second model has been developed where the gas phase dynamics is based just on a single-bubble size (SBCM). Both models take into account the recirculation in the gas and liquid phases. For the estimation of the levels of gas and liquid recirculation, a sub-model was developed to estimate the radial profiles of the axial time-averaged liquid and gas velocities. This sub-model is based on a simplification of the two-fluid equations for Eulerian description of multiphase flows; and the liquid-phase turbulence is closed by the modified mixing length closure from Kumar,

Devanathan, Moslemian and Dudukovic (1994). Details of the sub-model equations, method of solution and model parameter estimation from the solution of the sub-model equations have been discussed elsewhere (Gupta, Ong, Al-Dahhan, Dudukovic & Toseland, 2000).

2. Experiments

The experimental data for this study was obtained in a pilot-scale slurry bubble column reactor at the Department of Energy (DOE) facility at La Porte, Texas (AFDU). Radioactive gas tracer measurements were conducted using Ar^{41} in a 46-cm diameter slurry bubble column. The dispersed gas-slurry height was maintained at approximately 13.25 m with the chemical process being the liquid-phase synthesis of methanol from Syngas ($CO + H_2$). Fig. 1 shows the schematic of the
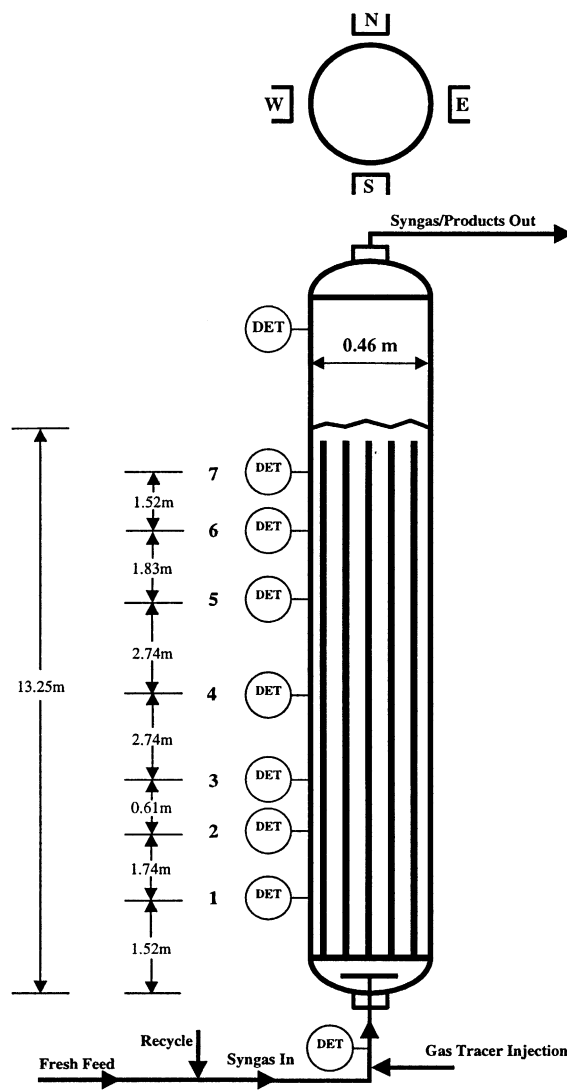

Fig. 1. Schematic of pilot-scale slurry bubble column reactor at the AFDU, La Porte.

Table 1
Estimated gas holdup profile for the three operating conditions during the gas tracer experiments

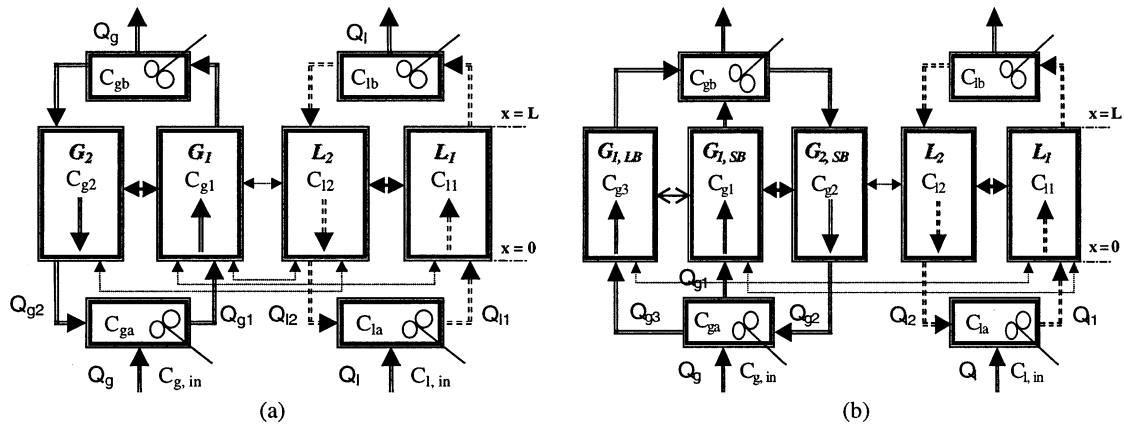| Experiment number	Pressure (MPa)	Temperature (°C)	$\bar{U}_{G,\text{sup}}$ (cm/s)	Parameters of the radial gas holdup profile		
				$\bar{\varepsilon}_g$	m	c
Run 14.6	5.27	250	22.9	0.39	2	0.844
Run 14.7	5.27	250	12.7	0.33	2	0.89
Run 14.8	3.63	250	32.8	0.37	2	0.943

Fig. 2. Schematic representation of bubble column reactor compartmentalization for: (a) single-bubble class model (SBCM); (b) two-bubble class model (TBCM).

experimental setup with the gas tracer injected below the sparger in the inlet Syngas stream. The temporal evolution of the tracer inside the reactor at three different operating conditions was measured using scintillation counters at seven different axial locations with four detectors at each level (see Fig. 1). To estimate the gas holdup distribution in the column, pressure-drop and nuclear density gauge (NDG) measurements were made along the column length. These measurements indicated that the gas holdup in the column was fairly constant except in the distributor and the free board regions. Table 1 shows the parameters in the estimated radial gas holdup profile at the three different operating conditions. The details of estimation of these parameters, detector calibration and experimental procedure can be found elsewhere (Degaleesan et al., 1996a; Degaleesan, 1997).

3. Mechanistic reactor models

The reactor compartmentalization for the SBCM is shown in Fig. 2a, whereas Fig. 2b shows the same for the TBCM. In both models, the gas phase is assumed to be recirculating along with the liquid/slurry. The slurry has been assumed to be pseudo-homogeneous for the purposes of this study. For the SBCM, the gas phase is

assumed to consist only of a single mean bubble size both in the core up-flow as well as the wall down-flow regions. For the TBCM on the other hand, the up-flowing gas in the core of the reactor is assumed to be made up of a lean "large" and a dense "small" bubble phases (de Swart, 1996), while the down-flowing gas in the annular region consists only of small bubbles which do not possess sufficient momentum and get recirculated with the down-flowing slurry. The model equations resulting from the two reactor models are presented in Table 2 and are the classical transient-convection–diffusion–reaction PDEs, one for each compartment in the well-developed regions; while the end-zones are modeled as continuous stirred tanks (CSTs) the dynamics of which are well-represented by ODEs. The estimation of the model parameters from a hydrodynamic sub-model based on gas–liquid recirculation (equations presented at the bottom of Table 2 and discussed in detail by Gupta et al., 2000) requires the knowledge of the radial gas holdup profile, which is frequently represented in terms of the following function and is known to fit the experimental data well (Kumar et al., 1994).

$$\varepsilon_g(\xi) = \bar{\varepsilon}_g \left(\frac{m+2}{m+2-2c} \right) (1 - c\xi^m). \qquad (1)$$

Table 2
Model equations for single-bubble class and two-bubble class models

Single-bubble class model	Two-bubble class model

Single-bubble class model

$$\frac{\partial C_{g1}}{\partial t} = \left\{ \begin{aligned} &\bar{D}_{xx_1}\frac{\partial^2 C_{g1}}{\partial x^2} - \bar{u}_{g1}\frac{\partial C_{g1}}{\partial x} - \frac{4(\bar{D}_{rr}\varepsilon_g)_{r=r''}}{r''R\bar{\varepsilon}_{g1}}(C_{g1}-C_{g2}) + R_{x,g1} \\ &- \frac{k_{gulu}a_{gulu}}{\bar{\varepsilon}_{g1}}(HC_{g1}-C_{l1}) - \frac{K_{guld}a_{guld}}{\bar{\varepsilon}_{g1}}(HC_{g1}-C_{l2}) \end{aligned} \right\}$$

$$\frac{\partial C_{g2}}{\partial t} = \left\{ \begin{aligned} &\bar{D}_{xx_2}\frac{\partial^2 C_{g2}}{\partial x^2} + \bar{u}_{g2}\frac{\partial C_{g2}}{\partial x} - \frac{k_{gdld}a_{gdld}}{\bar{\varepsilon}_{g2}}(HC_{g2}-C_{l2}) \\ &+ \frac{4r''/R}{R^2-r''^2}\frac{(\bar{D}_{rr}\varepsilon_g)_{r=r''}}{\bar{\varepsilon}_{g2}}(C_{g1}-C_{g2}) + R_{x,g2} \end{aligned} \right\}$$

$$\frac{\partial C_{l1}}{\partial t} = \left\{ \begin{aligned} &\bar{D}_{xx_1}\frac{\partial^2 C_{l1}}{\partial x^2} - \bar{u}_{l1}\frac{\partial C_{l1}}{\partial x} + \left(\frac{r''}{r'}\right)^2\frac{k_{gulu}a_{gulu}}{\bar{\varepsilon}_{l1}}(HC_{g1}-C_{l1}) \\ &- \frac{4(\bar{D}_{rr}\varepsilon_l)_{r=r'}}{r'R\bar{\varepsilon}_{l1}}(C_{l1}-C_{l2}) + R_{x,l1} \end{aligned} \right\}$$

$$\frac{\partial C_{l2}}{\partial t} = \left\{ \begin{aligned} &\bar{D}_{xx_2}\frac{\partial^2 C_{l2}}{\partial x^2} + \bar{u}_{l2}\frac{\partial C_{l2}}{\partial x} + \frac{4r'/R}{R^2-r'^2}\frac{(\bar{D}_{rr}\varepsilon_l)_{r=r'}}{\bar{\varepsilon}_{l2}}(C_{l1}-C_{l2}) \\ &+ \left(\frac{r''^2}{R^2-r'^2}\right)\frac{k_{guld}a_{guld}}{\bar{\varepsilon}_{l2}}(HC_{g1}-C_{l2}) \\ &+ \left(\frac{R^2-r''^2}{R^2-r'^2}\right)\frac{k_{gdld}a_{gdld}}{\bar{\varepsilon}_{l2}}(HC_{g2}-C_{l2}) \end{aligned} \right\}$$

$$\frac{dC_{ga}}{dt} = \left\{ \begin{aligned} &\frac{\bar{\varepsilon}_{g2}\bar{u}_{g2}}{\bar{\varepsilon}_g\phi_{in}D_C}\frac{(R^2-r''^2)}{R^2}C_{g2,0} - \frac{\bar{\varepsilon}_{g1}\bar{u}_{g1}}{\bar{\varepsilon}_g\phi_{in}D_C}\frac{r''^2}{R^2}C_{ga} \\ &+ \frac{U_G}{\bar{\varepsilon}_g\phi_{in}D_C}C_{g,in} - \frac{k_{CST}a_{CST}}{\bar{\varepsilon}_g}(HC_{ga}-C_{la}) + R_{x,ga} \end{aligned} \right\}$$

$$\frac{dC_{la}}{dt} = \left\{ \begin{aligned} &\frac{\bar{\varepsilon}_{l2}\bar{u}_{l2}}{\bar{\varepsilon}_l\phi_{in}D_C}\frac{(R^2-r'^2)}{R^2}C_{l2,0} - \frac{\bar{\varepsilon}_{l1}\bar{u}_{l1}}{\bar{\varepsilon}_l\phi_{in}D_C}\frac{r'^2}{R^2}C_{la} \\ &+ \frac{U_L}{\bar{\varepsilon}_l\phi_{in}D_C}C_{l,in} + \frac{k_{CST}a_{CST}}{\bar{\varepsilon}_l}(HC_{ga}-C_{la}) + R_{x,la} \end{aligned} \right\}$$

$$\frac{dC_{gb}}{dt} = \left\{ \begin{aligned} &\frac{\bar{\varepsilon}_{g1}\bar{u}_{g1}}{\bar{\varepsilon}_g\phi_{out}D_C}\frac{r''^2}{R^2}C_{g1,L} - \frac{\bar{\varepsilon}_{g2}\bar{u}_{g2}}{\bar{\varepsilon}_g\phi_{out}D_C}\frac{(R^2-r''^2)}{R^2}C_{gb} \\ &- \frac{U_G}{\bar{\varepsilon}_g\phi_{out}D_C}C_{gb} - \frac{k_{CST}a_{CST}}{\bar{\varepsilon}_g}(HC_{gb}-C_{lb}) + R_{x,gb} \end{aligned} \right\}$$

$$\frac{dC_{lb}}{dt} = \left\{ \begin{aligned} &\frac{\bar{\varepsilon}_{l1}\bar{u}_{l1}}{\bar{\varepsilon}_l\phi_{out}D_C}\frac{r'^2}{R^2}C_{l1,L} - \frac{\bar{\varepsilon}_{l2}\bar{u}_{l2}}{\bar{\varepsilon}_l\phi_{out}D_C}\frac{(R^2-r'^2)}{R^2}C_{lb} \\ &- \frac{U_L}{\bar{\varepsilon}_l\phi_{out}D_C}C_{lb} + \frac{k_{CST}a_{CST}}{\bar{\varepsilon}_l}(HC_{gb}-C_{lb}) + R_{x,lb} \end{aligned} \right\}$$

$$d_B = \bar{d}$$

Two-bubble class model

$$\frac{\partial C_{g1}}{\partial t} = \left\{ \begin{aligned} &\bar{D}_{xx_1}\frac{\partial^2 C_{g1}}{\partial x^2} - \bar{u}_{g1}\frac{\partial C_{g1}}{\partial x} - \left(\frac{4(\bar{D}_{rr}\varepsilon_g)_{r=r''}}{r''R\bar{\varepsilon}_{g1}} + \frac{K_{SB_1-LB}}{\bar{\varepsilon}_{g1}}\right)(C_{g1}-C_{g2}) \\ &- \frac{k_{sulu}a_{sulu}}{\bar{\varepsilon}_{g1}}(HC_{g1}-C_{l1}) - \frac{K_{suld}a_{suld}}{\bar{\varepsilon}_{g1}}(HC_{g1}-C_{l2}) + R_{x,g1} \end{aligned} \right\}$$

$$\frac{\partial C_{g2}}{\partial t} = \left\{ \begin{aligned} &\bar{D}_{xx_2}\frac{\partial^2 C_{g2}}{\partial x^2} + \bar{u}_{g2}\frac{\partial C_{g2}}{\partial x} - \frac{k_{sdld}a_{sdld}}{\bar{\varepsilon}_{g2}}(HC_{g2}-C_{l2}) \\ &+ \frac{4r''/R}{R^2-r''^2}\frac{(\bar{D}_{rr}\varepsilon_g)_{r=r''}}{\bar{\varepsilon}_{g2}}(C_{g1}-C_{g2}) + R_{x,g2} \end{aligned} \right\}$$

$$\frac{\partial C_{g3}}{\partial t} = \left\{ -\bar{u}_{g3}\frac{\partial C_{g3}}{\partial x} - \frac{k_l a_l}{\bar{\varepsilon}_{g3}}(HC_{g3}-C_{l1}) + \frac{K_{SB_1-LB}}{\bar{\varepsilon}_{g3}}(C_{g1}-C_{g3}) \right\}$$

$$\frac{\partial C_{l1}}{\partial t} = \left\{ \begin{aligned} &\bar{D}_{xx_1}\frac{\partial^2 C_{l1}}{\partial x^2} - \bar{u}_{l1}\frac{\partial C_{l1}}{\partial x} - \frac{4(\bar{D}_{rr}\varepsilon_l)_{r=r'}}{r'R\bar{\varepsilon}_{l1}}(C_{l1}-C_{l2}) + R_{x,l1} \\ &+ \left(\frac{r''}{r'}\right)^2\frac{1}{\bar{\varepsilon}_{l1}}[k_{sulu}a_{sulu}(HC_{g1}-C_{l1}) + k_l a_l(HC_{g3}-C_{l1})] \end{aligned} \right\}$$

$$\frac{\partial C_{l2}}{\partial t} = \left\{ \begin{aligned} &\bar{D}_{xx_2}\frac{\partial^2 C_{l2}}{\partial x^2} + \bar{u}_{l2}\frac{\partial C_{l2}}{\partial x} + \frac{4r'/R}{R^2-r'^2}\frac{(\bar{D}_{rr}\varepsilon_l)_{r=r'}}{\bar{\varepsilon}_{l2}}(C_{l1}-C_{l2}) \\ &+ \left(\frac{r''^2}{R^2-r'^2}\right)\frac{k_{suld}a_{suld}}{\bar{\varepsilon}_{l2}}(HC_{g1}-C_{l2}) \\ &+ \left(\frac{R^2-r''^2}{R^2-r'^2}\right)\frac{k_{sdld}a_{sdld}}{\bar{\varepsilon}_{l2}}(HC_{g2}-C_{l2}) \end{aligned} \right\}$$

$$\frac{dC_{ga}}{dt} = \left\{ \begin{aligned} &\frac{\bar{\varepsilon}_{g2}\bar{u}_{g2}}{\bar{\varepsilon}_g\phi_{in}D_C}\frac{(R^2-r''^2)}{R^2}C_{g2,0} - \frac{(\bar{\varepsilon}_{g1}\bar{u}_{g1}+\bar{\varepsilon}_{g3}\bar{u}_{g3})}{\bar{\varepsilon}_g\phi_{in}D_C}\frac{r''^2}{R^2}C_{ga} \\ &+ \frac{U_G}{\bar{\varepsilon}_g\phi_{in}D_C}C_{g,in} - \frac{k_{CST}a_{CST}}{\bar{\varepsilon}_g}(HC_{ga}-C_{la}) + R_{x,ga} \end{aligned} \right\}$$

$$\frac{dC_{la}}{dt} = \left\{ \begin{aligned} &\frac{\bar{\varepsilon}_{l2}\bar{u}_{l2}}{\bar{\varepsilon}_l\phi_{in}D_C}\frac{(R^2-r'^2)}{R^2}C_{l2,0} - \frac{\bar{\varepsilon}_{l1}\bar{u}_{l1}}{\bar{\varepsilon}_l\phi_{in}D_C}\frac{r'^2}{R^2}C_{la} \\ &+ \frac{U_L}{\bar{\varepsilon}_l\phi_{in}D_C}C_{l,in} + \frac{k_{CST}a_{CST}}{\bar{\varepsilon}_l}(HC_{ga}-C_{la}) + R_{x,la} \end{aligned} \right\}$$

$$\frac{dC_{gb}}{dt} = \left\{ \begin{aligned} &\frac{\bar{\varepsilon}_{g1}\bar{u}_{g1}}{\bar{\varepsilon}_g\phi_{out}D_C}\frac{r''^2}{R^2}C_{g1,L} + \frac{\bar{\varepsilon}_{g3}\bar{u}_{g3}}{\bar{\varepsilon}_g\phi_{out}D_C}\frac{r''^2}{R^2}C_{g3,L} - \frac{U_G}{\bar{\varepsilon}_g\phi_{out}D_C}C_{gb} \\ &- \frac{\bar{\varepsilon}_{g2}\bar{u}_{g2}}{\bar{\varepsilon}_g\phi_{out}D_C}\frac{(R^2-r''^2)}{R^2}C_{gb} - \frac{k_{CST}a_{CST}}{\bar{\varepsilon}_g}(HC_{gb}-C_{lb}) + R_{x,gb} \end{aligned} \right\}$$

$$\frac{dC_{lb}}{dt} = \left\{ \begin{aligned} &\frac{\bar{\varepsilon}_{l1}\bar{u}_{l1}}{\bar{\varepsilon}_l\phi_{out}D_C}\frac{r'^2}{R^2}C_{l1,L} - \frac{\bar{\varepsilon}_{l2}\bar{u}_{l2}}{\bar{\varepsilon}_l\phi_{out}D_C}\frac{(R^2-r'^2)}{R^2}C_{lb} \\ &- \frac{U_L}{\bar{\varepsilon}_l\phi_{out}D_C}C_{lb} + \frac{k_{CST}a_{CST}}{\bar{\varepsilon}_l}(HC_{gb}-C_{lb}) + R_{x,lb} \end{aligned} \right\}$$

$$d_B = \bar{d}_{G_{1,LB}}(1-c\xi^m)$$

Hydrodynamic model

$$\varepsilon_g(\xi) = \bar{\varepsilon}_g\left(\frac{m+2}{m+2-2c}\right)(1-c\xi^m)$$

Liquid phase

$$0 = -(\rho_g\varepsilon_g + \rho_l\varepsilon_l)g - \frac{dP}{dz} + \frac{1}{r}\frac{d}{dr}(r\varepsilon_l\tau_{l,rz})$$

$$\tau_{l,rz}(\xi) = -\frac{\rho_l v_t^m}{R}\frac{du_l}{d\xi} - \frac{\rho_l l^2}{R^2}\left(\frac{du_l}{d\xi}\right)^2$$

$$\frac{l(\xi)}{R} = \frac{a(1-\xi)}{(\xi+b)^c} + d(1-\xi)^c \qquad \text{Kumar et al. (1994)}$$

Gas phase

$$0 = -\rho_g\varepsilon_g g - \varepsilon_g\frac{dP}{dz} + M_d$$

$$M_d = -\frac{3\varepsilon_l\varepsilon_g\rho_l C_D}{4d_B}(u_l-u_g)^2$$

$$C_D = \max\left[\frac{24}{Re}(1+0.15Re^{0.687}), \frac{8}{3}\frac{Eo}{Eo+4}\right]$$

Tomiyama, Kataoka and Sakaguchi (1995)

The radial distribution of the effective mean bubble-size (Eq. (2)) is obtained as part of the solution of the sub-model equations by satisfying the gas-phase continuity in the computation of the gas velocity profile.

$$d(\xi) = \begin{cases} \bar{d} & \text{for use in SBCM} \\ \bar{d}_{G_{1,LB}} \ (1 - c\xi^m) & \text{for use in TBCM} \end{cases} \quad (2)$$

Thus, the *effective mean* bubble-size is a constant for SBCM ($\bar{d}$), while for TBCM it is assumed to have a radial distribution represented by Eq. (2), where $\bar{d}_{G_{1,LB}}$ is the effective mean diameter of the "large" bubble phase and is obtained as part of the solution of the sub-model equations for estimating gas and liquid recirculation velocities. The effective mean bubble diameter of the "small" bubbles in TBCM is estimated from Eqs. (4) and (6) as shown later. This assumed distribution of the *effective mean* bubble diameter is justified in view of the similarity with the radial gas holdup profile with a relatively flat radial gas holdup profile implying that the *effective mean* bubble size is homogeneous. On the other hand, a large gradient in the radial gas holdup implies greater concentration of gas in the column center resulting in relatively larger bubble voids coexisting with smaller sized bubbles, and only the "small" bubble phase present in the annular region. Therefore, this assumption on radial distribution of long-time-averaged bubble size automatically reflects the non-uniformity in the radial gas holdup profile.

Fig. 3 exhibits the radial profiles of the axial time-averaged liquid/slurry and gas velocity profiles computed from the hydrodynamic sub-model for the three operating conditions listed in Table 1. Convergence on gas phase continuity is achieved by iterating on $\bar{d}$ for SBCM and $\bar{d}_{G_{1,LB}}$ for TBCM. Clearly the computed gas velocity profile is not significantly affected by the nature of the radial distribution of the mean effective bubble diameter. In addition, the slip velocity between the gas and slurry phases could be as high as 50–60 cm/s in the column center depending on the superficial gas velocity. Based on these converged liquid & gas velocity profiles, the converged *effective mean* bubble size profile, and the known radial gas holdup profile, all the model parameters for the SBCM can be evaluated as shown by Gupta et al. (2000). However for the TBCM, additional estimation of the mean small bubble sizes in the core and annular regions ($\bar{d}_{G_{1,SB}}$ & $\bar{d}_{G_{2,SB}}$, respectively) is required as discussed below. From Eqs. (1) and (2), a bubble number density function defined as number of bubbles per unit reactor cross-sectional area is obtained:

$$n_B(\xi) = \frac{4\varepsilon_g(\xi)}{\pi d_B^2(\xi)}. \quad (3)$$

From Eq. (3), the following quantities are estimated by averaging over the core and annular regions, the boundary between which is denoted by ξ'' (the dimensionless
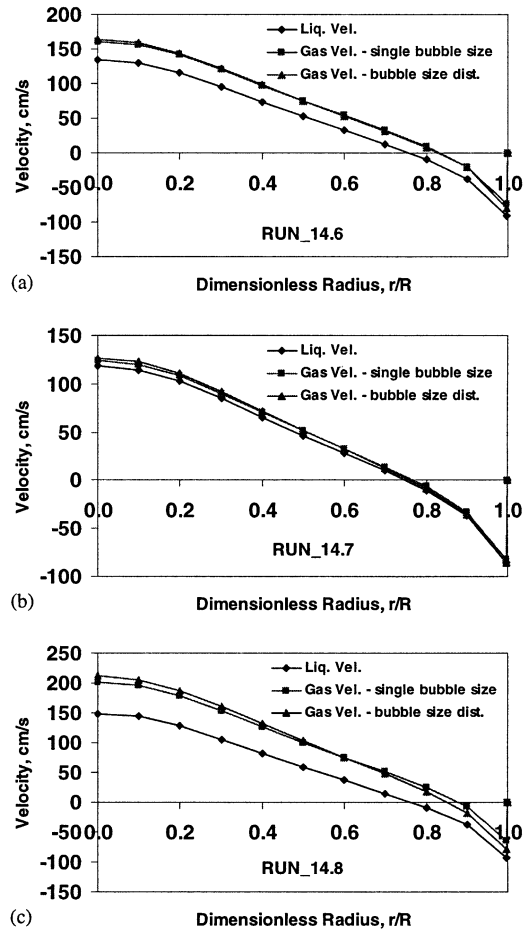

Fig. 3. Liquid and gas radial velocity profiles for the three different operating conditions.

radius where gas velocity becomes zero).

$$\bar{n}_{G_{2,SB}} = \frac{2}{(1 - \xi''^2)} \int_{\xi''}^{1} n_B(\xi)\xi \,\mathrm{d}\xi \Rightarrow \bar{d}_{G_{2,SB}} = \sqrt{\frac{4\bar{\varepsilon}_{g2}}{\pi \bar{n}_{G_{2,SB}}}}, \quad (4)$$

$$\bar{n}_{G_{1,SB+LB}} = \frac{2}{\xi''^2} \int_{0}^{\xi''} n_B(\xi)\xi \,\mathrm{d}\xi \Rightarrow \bar{d}_{G_{1,SB+LB}} = \sqrt{\frac{4(\bar{\varepsilon}_{g1} + \bar{\varepsilon}_{g3})}{\pi \bar{n}_{G_{1,SB+LB}}}}. \quad (5)$$

In the above set of equations, the subscript "$G_{1,SB+LB}$" refers to the small and large bubbles in the core. By assuming *holdups of the small bubbles in the core and annulus to be equal* for TBCM, it implies that $\bar{n}_{G_{1,SB}} \bar{d}_{G_{1,SB}}^2 = \bar{n}_{G_{2,SB}} \bar{d}_{G_{2,SB}}^2$. With this assumption, the mean diameter of the small bubbles in the core is calculated as

$$\bar{n}_{G_{1,LB}} = \frac{\bar{n}_{G_{1,SB+LB}} \bar{d}_{G_{1,SB+LB}}^2 - \bar{n}_{G_{2,SB}} \bar{d}_{G_{2,SB}}^2}{\bar{d}_{G_{1,LB}}^2},$$

$$\bar{d}_{G_{1,SB}} = \sqrt{\frac{\bar{n}_{G_{2,SB}} \bar{d}_{G_{2,SB}}^2}{(\bar{n}_{G_{1,SB+LB}} - \bar{n}_{G_{1,LB}})}}. \quad (6)$$

Table 3 lists the estimated mean bubble sizes at the three operating conditions for both reactor models. Knowing the mean "small" and "large" bubble diameters in the core, the mass transfer coefficients and specific interfacial areas for these two bubble phases are estimated in a similar manner as for the SBCM (Gupta et al., 2000). Once all the hydrodynamic parameters for the two reactor models are estimated by the procedure described above, the reactor model equations are solved by a fully implicit finite difference scheme which is robust and does not present problems related to stability and convergence.

4. Simulation comparison with experimental data

Figs. 4–7 present the comparison of the normalized experimental tracer response curves (detector level 7) with simulated responses computed from the two reactor models discussed above. The purpose of this is to evaluate the effect of some of the key model parameters as well as to compare the two models against each other in their ability to predict tracer responses. From Fig. 4, one can see that the effect of the axial dimension of the distributor and disengagement CSTs on the simulated tracer responses is negligible for both SBCM as well as TBCM. This result is similar to that of Degaleesan et al. (1996b) for liquid mixing studies in both laboratory as well as pilot-scale columns. Thus, for all subsequent simulations (Figs. 5–7), the height of these regions was set to one column diameter.

The important parameters that affect the spread of the gas-phase tracer response curves are the Henry's constant and the volumetric mass transfer coefficients. As was shown by Degaleesan et al. (1996a), the tracer response curves simulated using the ADM were also very sensitive to these two parameters, however, no consistent trend was found in their estimated values. Fig. 5 presents the comparison of the simulated and experimental responses for several values of the Henry's constant, which is *dimensionless* and is defined as the ratio of the concentration of Argon in the liquid to that in the gas when the two phases are in equilibrium. One can see from this figure that for both the SBCM as well as for the TBCM, the value of the Henry's constant can significantly affect the peak arrival time, since a larger value of the Henry's constant implies that the tracer stays longer in the liquid/slurry phase resulting in a prolonged residence time. Except for Run 14.8, the simulated tracer curves based on the thermodynamically estimated value of the Henry's constant (H^*) result in excellent match of the peak time of the experimental curves with under estimation of the spreads in the tracer response curves about these peaks. It should, however, be noted that the measured tracer responses are a result of radiation measurement, which leads to additional broadening of the tracer curves due to practical limitations on detector shielding in a pilot-scale set-up. The relatively poor prediction for Run 14.8 could be attributed to the relatively larger bubble sizes, which lead to a significantly lower mass transfer between the gas and the liquid.

Fig. 6 examines the effect of the small and large bubble interaction parameter for the TBCM. It can be seen from the figure that the intensity of bubble–bubble interactions has a significant effect on the tracer curve only for an insoluble gas ($H = 0$). On the other hand, there is a negligible effect of the intensity of bubble–bubble interactions, expressed through the exchange coefficient, on tracer responses particularly at theoretical solubility value. It should however be kept in mind that the average speeds at which the "small" and "large" bubbles travel do not differ by more than 30–45 cm/s as computed from the parameter estimation procedure. It is possible, therefore,

Table 3
Estimated mean bubble sizes for SBCM and TBCM at the three operating conditions

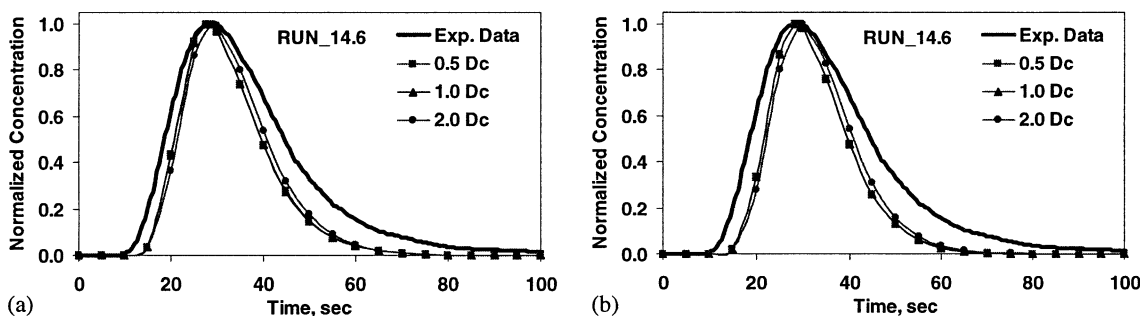| Run number	SBCM		TBCM	
	$\bar{d}$ (mm)	$\bar{d}_{G_{1,LB}}$ (mm)	$\bar{d}_{G_{1,SB}}$ (mm)	$\bar{d}_{G_{2,SB}}$ (mm)
14.6	6.07	8.1	4.5	2.6
14.7	0.39	0.55	0.31	0.15
14.8	26.55	38.67	18.56	8.54

Fig. 4. Effect of the axial dimension of the distributor and disengagement CSTs on the simulated gas tracer response curves computed using: (a) SBCM; (b) TBCM.
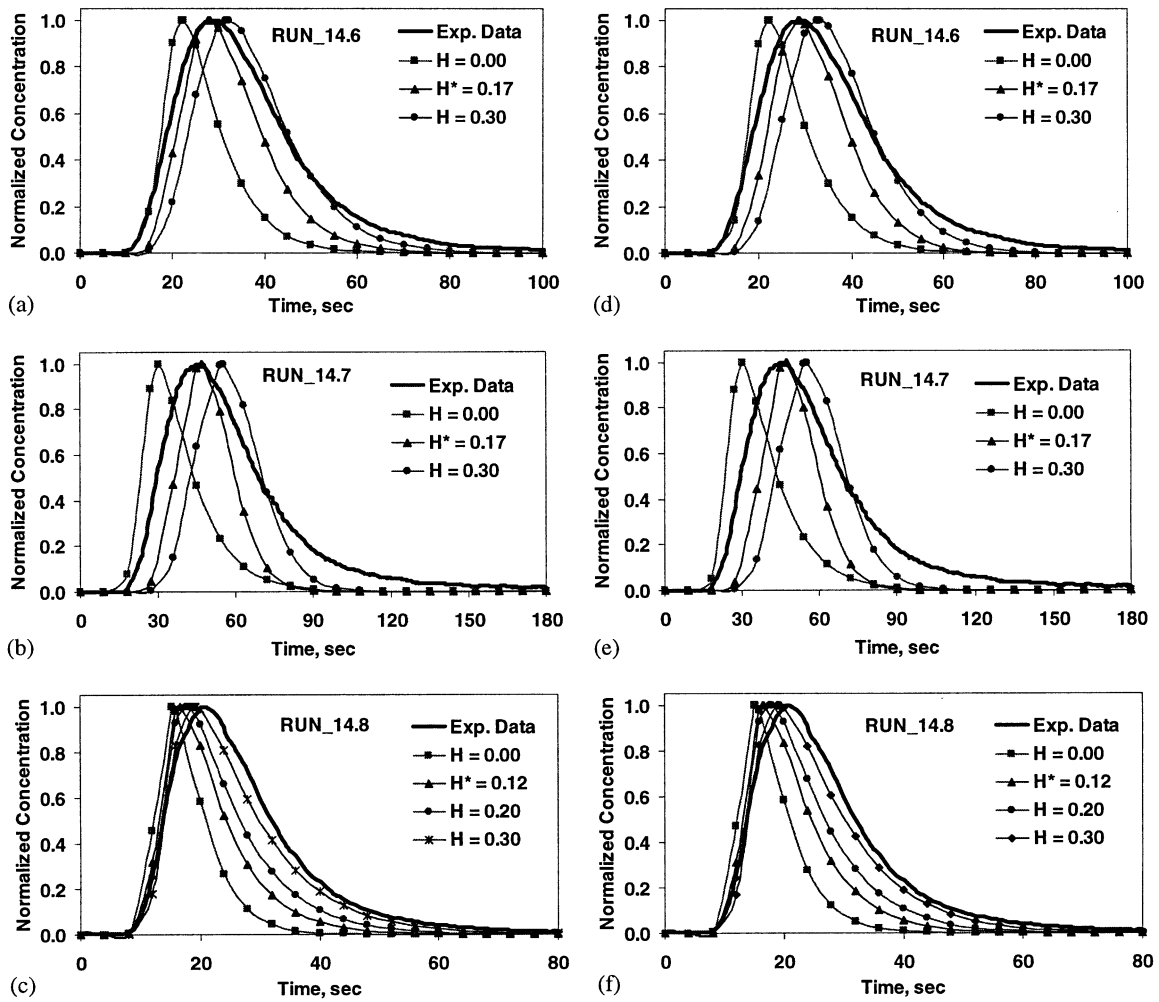
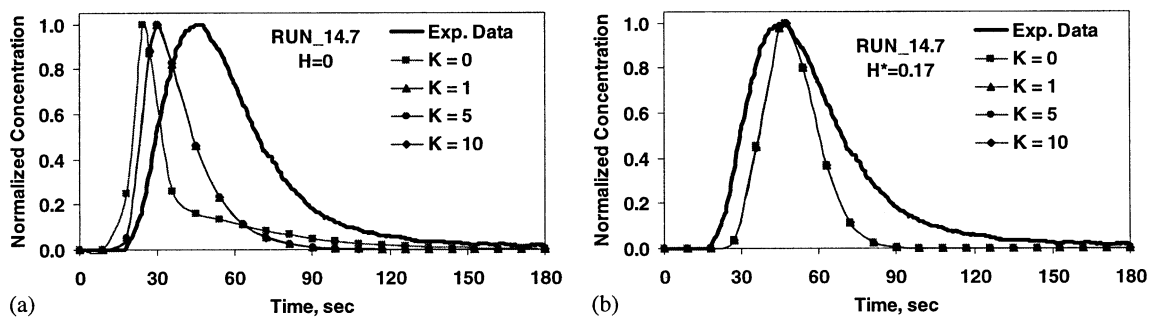Fig. 5. Effect of Henry's constant on simulated gas-tracer response curves: (a)–(c) SBCM; (d)–(f) TBCM.

Fig. 6. Effect of bubble-interaction parameter on simulated response curves (Run_14.7): (a) $H = 0$; (b) $H = H^*$.

that the velocities of the "small" and "large" bubble phases differ much more than assumed here, if computed using literature correlations (Krishna & Ellenberger, 1996). In that case, the bubble–bubble interaction parameter, K (1/s) would have a more pronounced effect on the simulated tracer responses. However, many such correla-

tions for bubble rise are developed without consideration of the inherent recirculatory nature of the flow, and may not provide good estimates for the bubble velocities.

The last effect evaluated in this study is the assumption of the existence of two-bubble classes. Fig. 7 presents the result of such comparison, where the simulated responses
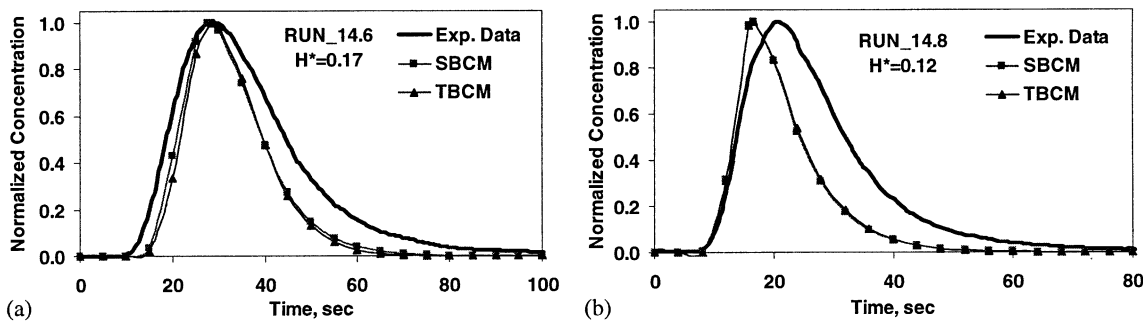
Fig. 7. Comparison of simulated tracer response curves from SBCM and TBCM with experimental data: (a) Run 14.6; (b) Run 14.8.

have been computed using $K = 10$ 1/s. One can see from this figure that the two models do not exhibit any significant differences as far as comparison with tracer response data is concerned. This result is not too surprising as the "small" and "large" bubble-phase equations for the TBCM when added together result in the equation describing the dynamics of the up-flowing gas in the SBCM. Therefore, one does not really need to make the assumptions about the bi-disperse bubble-size distribution to characterize the gas-phase dynamics, as long as a reasonably accurate description of the recirculation in the gas and liquid-phases is incorporated into the reactor model.

5. Concluding remarks

The comparison of the simulation results with gas tracer experiments reported in an earlier study (Degaleesan et al., 1996a) indicates that the TBCM does not present additional benefits over the SBCM. The TBCM does have an additional bubble–bubble interaction parameter, which has an effect on the gas phase tracer responses only in the absence of gas–liquid mass transfer. Coupled with a proper estimation of mass transfer effects, the simulated tracer responses are found to be in reasonable agreement with experimental data; indicating reliable predictability from the solution of the model equations. Further, with incorporation of the reaction kinetics, these models provide the rational tools for scale-up and prediction of reactor performances.

Notation

a	interfacial area, 1/cm
c	parameter in hold-up profile
C	concentration, mole/cm^3
C_D	drag coefficient
D_C	column diameter, cm
d	mean bubble diameter, cm
$D_{L,m}$	molecular diffusivity, cm^2/s
$\bar{D}_{rr}$	radial turbulent diffusivity, cm^2/s
$\bar{D}_{xx}$	axial turbulent diffusivity, cm^2/s
E_o	Eotvos number
g	acceleration due to gravity, cm^2/s
H	Henry's constant
k	mass transfer coefficient, cm/s
K	exchange coefficient, 1/s
l	mixing length, cm
L	dispersion height, cm
m	exponent in hold-up profile
Q	flow rate, cm^3/s
R	column radius, cm
R_x	reaction rate, mol/cm^3/s
t	time, s
$\bar{U}_{G,\text{sup}}$	gas superficial velocity, cm/s
u	velocity, cm/s
$\bar{u}$	radially averaged mean velocity, cm/s
V	volume of end zone CSTs, cm^3
x	axial position in the column, cm

Greek letters

ε	local phase hold-up
$\bar{\varepsilon}_g$	radially averaged phase hold-up
ϕ	fraction of the column diameter
ρ	density, g/cm^3
σ	surface tension of the liquid, dyn/cm
$\tau_{l,rz}$	total shear stress, dyn/cm^2
v^m	kinematic viscosity, cm^2/s
ξ	dimensionless radius
ξ'	liquid velocity inversion point
ξ''	gas velocity inversion point

References

Chen, J., Gupta, P., Degaleesan, S., Al-Dahhan, M.H., Dudukovic', M.P., & Toseland, B.A. (1998). Gas holdup distributions in large-diameter bubble columns measured by computed tomography. *Flow Measurement and Instrumentation, 9*, 91–101.

Degaleesan, S., & Dudukovic, M. P. (1998). Liquid backmixing in bubble columns and the axial dispersion coefficient. *A.I.Ch.E. Journal, 44* (11), 2369–2378.

Degaleesan, S. (1997). *Fluid dynamic measurements and modeling of liquid mixing in bubble columns*. D.Sc. thesis, Washington University.

Degaleesan, S., Dudukovic', M. P., Bhatt, B. L., & Toseland, B. A. (1996a). Slurry bubble column hydrodynamics: Tracer studies of the La Porte AFDU Reactor during methanol synthesis. *Fourth quarterly report for Contract DOE-FC 2295 PC 95051*.

Degaleesan, S., Roy, S., Kumar, S. B., & Dudukovic', M. P. (1996b). Liquid backmixing based on convection and turbulent dispersion in bubble columns. *Chemical Engineering Science, 51*, 1967–1976.

Devanathan, N., Moslemian, D., & Dudukovic', M. P. (1990). Flow mapping in bubble columns using CARPT. *Chemical Engineering Science, 45*, 2285–2291.

Gupta, P., Ong, B., Al-Dahhan, M. H., Dudukovic, M. P., & Toseland, B. A. (2000). Hydrodynamics of Churn-Turbulent Bubble Columns: Gas–Liquid Recirculation and Mechanistic Modeling. Accepted for publication in a topical issue of *Catalysis Today*.

Kastanek, F., Zahradnik, J., Kratochvil, J., & Cermak, J. (1993). *Chemical reactions for gas–liquid systems*. New York: Ellis Horwood.

Krishna, R., & Ellenberger, J. (1996). Gas holdup in bubble column reactors operating in the churn-turbulent flow regime. *A.I.Ch.E. Journal, 42*, 2627–2634.

Kumar, S. B., Devanathan, N., Moslemian, D., & Dudukovic', M. P. (1994). Effect of scale on liquid recirculation in bubble columns. *Chemical Engineering Science, 49* (24B), 5637–5652.

Kumar, S. B., Moslemian, D., & Dudukovic, M. P. (1997). Gas holdup measurements in bubble columns using computed tomography. *A.I.Ch.E. Journal, 43* (6), 1414–1425.

Shah, Y. T., Kelkar, B. G., Godbole, S. P., & Deckwer, W. D. (1982). Design parameters estimation for bubble column reactors. *A.I.Ch.E. Journal, 28*, 353–379.

de Swart, J. W. A. (1996). Scale-up of a Fischer–Tropsch slurry reactor. Ph.D. thesis, University of Groningen, The Netherlands.

Tomiyama, A., Kataoka, I., & Sakaguchi, T. (1995). Drag coefficients of bubbles (1st report, drag coefficients of a single bubble in a stagnant liquid). *Transactions of the JSME Part B, 61* (587), 2357–2364.

Vermeer, D. J., & Krishna, R. (1981). Hydrodynamics and mass transfer in bubble columns operating in the churn-turbulent regime. *Industrial Engineering, Chemical Process Design and Development, 20*, 475–482.